Earth and Planetary Science Letters, 94 (1989) 316–328
Elsevier Science Publishers B.V., Amsterdam – Printed in The Netherlands

Fission-track analysis of basement apatites at the western margin of the Gulf of Suez rift, Egypt: evidence for synchroneity of uplift and subsidence

Gomaa I. Omar[1], Michael S. Steckler[2], W. Roger Buck[2] and Barry P. Kohn[3]

[1]*Department of Geology, University of Pennsylvania, Philadelphia, PA 19104 (U.S.A.)*
[2]*Lamont-Doherty Geological Observatory, Palisades, NY 10964 (U.S.A.)*
[3]*Department of Geology, Ben Gurion University, Beer Sheva 84105 (Israel)*

Received September 12, 1988; revised version received June 16, 1989

Fifty-six apatite fission-track ages and 52 horizontal confined track-length measurements are reported from Precambrian crystalline rocks along the western margin of the Gulf of Suez, Egypt. Ages fall in the range of ca. 11–385 m.y. and older ages often occur within very close geographic proximity to younger ones, indicating non-uniform uplift. The wide range in ages is accompanied by a systematic variation in the distribution of horizontal confined fission track lengths.

On the basis of apatite fission track ages and their length distributions, data fall into three distinct groups. Group I: ages ranging from 43 to 385 m.y. Length distributions are all positively skewed and with decreasing age become progressively broader with shorter mean track length. Group II: ages ranging from 23 to 31 m.y. Length distributions are negatively skewed with either a distinct tail or a small peak of short tracks. Group III: ages ranging from 11 to 20.5 m.y. Length distributions are al unimodal, narrow, negatively skewed and have the longest mean lengths among samples studied. Apatite ages from groups I and II are interpreted as "mixed ages" as a result of cooling during uplift from different levels within the apatite partial track annealing zone. Ages from Group III are interpreted as "cooling ages" due to uplift from the apatite total track annealing zone with minor partial annealing. Correcting the ages of the two oldest samples in this group for track-length reduction yields ages of 21 ± 2.2 and 23 ± 1.5 m.y. It is proposed that the onset of rift-flank uplift in the Gulf of Suez–northern Red Sea area occurred between 21 and 23 m.y. ago.

Fission-track analysis in combination with subsidence data from the Gulf of Suez basin, indicate that commencement of basement uplift postdate the start of rifting and is interpreted as evidence for passive rifting at the Gulf of Suez. Furthermore, this uplift is contemporaneous with, and is directly related to, the process of extension and subsidence at the Gulf of Suez.

1. Introduction

The Red Sea, a Neogene rift basin, bifurcates at its northern end at the Sinai Triple Junction (STJ) into the Gulf of Suez and the Gulf of Aqaba (inset Fig. 1). Among the three STJ branches, the Gulf of Suez has offered much of the available data base concerning the evolution of the northern Red Sea region. This is mainly because it has been a relatively shallow water marine basin which many hydrocarbon exploration wells have penetrated. Its subsidence history is, therefore, well documented [1–3].

In addition to subsidence in the rift basin, the flanks of the Gulf of Suez, as in many young rifts, are characterized by basement uplift parallel to its margins. However, little is known about the uplift history of these persistent basement highs. Elucidation of the uplift history is crucial to the understanding of the thermal evolution of the rift which in turn can be used to test theoretical models proposed for rift genesis. Information about the uplift history of these basement highs can be provided by fission track (FT) analysis. Application of FT analysis studies on apatite, age and horizontal confined track-length measurements, has proven to be an invaluable tool in determining tectono-thermal histories of basement uplift flanking rifted margins (e.g. [4–6]). FT analysis is par-

* L-DGO Contribution No. 4478.

0012-821X/89/$03.50

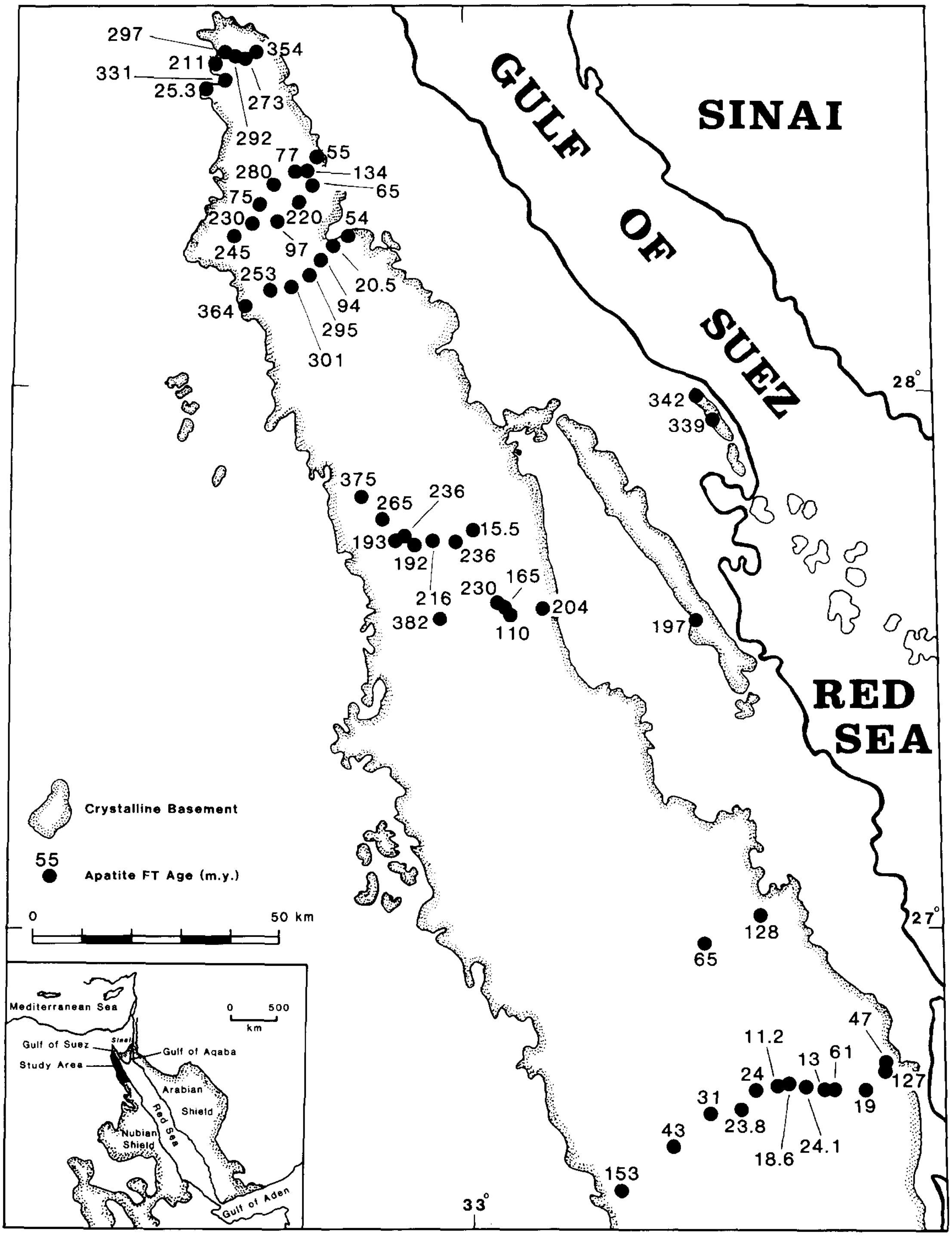

Fig. 1. Map showing the geographical distribution of apatite fission-track ages. Sample numbers and elevations may be read from Table 1. Sample coordinates are listed in Appendix 1.

ticularly useful in areas where the sedimentary cover on the basement is almost entirely eroded (as is the case in this study) thus precluding the use of conventional stratigraphic-structural methods for determining the uplift history of the basement rocks.

The western margin of the Gulf of Suez is an ideal setting for a FT study because its uplift history is not complicated by Gulf of Aqaba-Dead Sea transform tectonism as is the case in Sinai. Also, the basement complex has behaved as a tectonically stable platform since the Paleozoic, hence any significant vertical movement of the Gulf shoulder is rift-related.

The specific aims of this study are: (1) to use FT analysis on apatites to establish the geometry, timing and amount of rift-related basement uplift flanking the Gulf of Suez, and (2) to investigate the relationship between the uplift history and reported subsidence and extension histories of the rift basin; a relationship which when obtained can be used to place quantitative constraints on models for the uplift and subsidence of a rift. This report forms part of an ongoing fission track study of the basement complex along the western margin of the Red Sea in Egypt and Sudan.

2. Geological history

The oldest Precambrian rocks of the Arabo-Nubian shield comprise a metamorphic complex which underwent several phases of deformation. The complex was extensively intruded by two magmatic cycles (granitic-granodioritic in composition) each accompanied by extrusive activity [7]. Cratonization of the shield terminated at the end of Precambrian–early Paleozoic time, when the basement was uplifted and deeply eroded, resulting in the formation of a widespread peneplain extending over the Arabo-Nubian shield. The peneplained basement was overlain by the largely unfossiliferous early Cambrian to late Cretaceous sediments collectively known as the "Nubian Sandstone". A carbonate shelf platform developed over the Nubian Sandstone in the late Cretaceous and persisted into middle to late Eocene [7]. The Cretaceous to Eocene section comprises the southward thinning, coastal plain wedge of the neo-Tethyan Mediterranean continental margin.

The patchy occurrence of non-marine Oligocene sediments in the northern Eastern Desert of Egypt (area between the Nile and Red Sea–Gulf of Suez) and western Sinai, has been cited as evidence for Oligocene updoming preceding rifting. However, there is little evidence for erosion of an uplifted dome and the full thickness of pre-rift sediments is found below the syn-rift rocks except at local fault block highs [8,9]. This pattern of occurrence has also been interpreted as a major post-Eocene northward regional regression [10,11] probably related to the mid-Oligocene sea level fall [12,13].

In contrast to the isolated deposits of Oligocene synrift rocks, the Nukhul Formation is the first widespread synrift sedimentary unit in the area of the Gulf of Suez. It attains a thicknesses of up to 200–300 m. It usually consists of sandstone, sandy limestone, marl, shale and evaporites and contains marine fauna in its upper part [8,9]. Further, it contains beds and lenses of Eocene chert and limestone pebbles, with boulder-size conglomerates reported in a few places [8,9]. The upper Nukhul Formation is of Aquitanian age to Lower Burdigalian age (ca. 19–23 m.y. [8,9,14]). However, its base is poorly dated and could extend into the Oligocene. Thus by the end of Oligocene/earliest Miocene, rifting in the Gulf of Suez–Red Sea was underway [8].

The overlying Rudeis Formation (Late Burdigalian) expresses a shift to open marine deposition by a thick sequence of shale and globigerina marl with interbedded sandstones. The time interval represented by the Rudeis Formation is characterized by a dramatic increase in the rate of sediment accumulation [2,3] and water depths in parts of the rift basin which may have been as great as 200–500 m (upper bathyal [15]).

The subsequent Kareem Formation (Langhian) shows an increase in the amount of carbonates, and deposition evidently occurred in a shallow water environment [3,6]. During the Middle Miocene (Belayim Formation), intermittent evaporitic conditions in the Gulf prevailed as a result of the developing isolation of the rift basin from the Mediterranean Sea. Extensive evaporite deposition continued throughout the Late Miocene. A return to normal marine conditions occurred with the opening of a portal to the Indian Ocean at the close of the Miocene.

As mentioned above, the Nukhul Formation and few Oligocene rocks represent the early development of the Gulf of Suez rift. Steckler et al. [2] indicated that only few kilometers of extension occurred during the time period represented by these formations. The Rudeis Formation, in con-

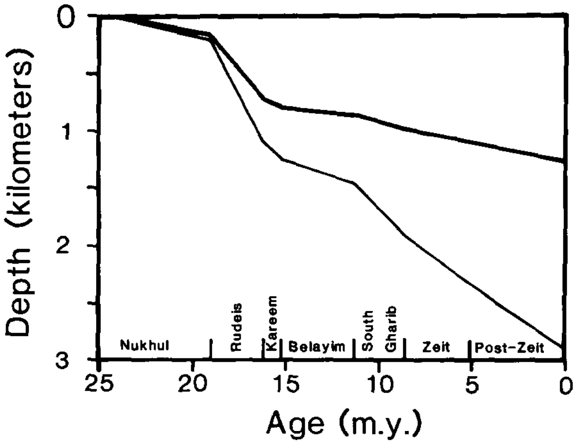

Fig. 2. Plot of average subsidence through time integrated from a transect across the Gulf of Suez rift centered at 28° N. The thin line (lower) represents the average sediment accumulation through time and the thick line (upper) shows the average tectonic subsidence estimated by backstripping profile.

trast, marks the beginning of much more rapid extension in the Gulf of Suez (at least 4–6 mm/yr). This phase of development encompasses at least 30–50% of total extension in the rift within only a few million years. By the end of Kareem Formation deposition (14–15 m.y.), the Gulf of Aqaba–Dead Sea transform had supplanted the Gulf of Suez as the primary plate boundary at the northern end of the Red Sea [17] and the subsidence rate in the Gulf of Suez greatly decreased. This three-phase evolution of the rift can clearly be seen in the tectonic subsidence calculated over a profile across the Gulf of Suez (Fig. 2).

Few magmatic events occurred in the northern Eastern Desert of Egypt during the Phanerozoic. Magmatism is represented by Wadi Dib ring complex (554 m.y. K-Ar [18]) and isolated dikes and sills near the margin of the Gulf of Suez [7]. The few reliable isotopic ages available for these bodies are of Oligocene–Miocene age [19].

The crystalline basement is exposed in the Eastern Desert from the central Gulf of Suez southwards. The outcrop forms a triangular shape, widening to the south, with a maximum width of about 75 km (Fig. 1). One reason for the outcrop pattern is that the prerift sedimentary cover thins to the south. Also, the amount of extension in the rift increases southwards. The sedimentary cover has been removed by scarp retreat, and the Eocene carbonates form a north–south escarpment beginning from the coast in the northern Gulf of Suez and diverging to about 100 km inland to the south. The exposed basement itself is rugged with elevations generally in the range of 300–800 m with numerous peaks exceeding 1000 m up to a maximum of over 1900 m.

3. Analytical techniques

Eighty samples of predominately dioritic and granodioritic compositions were collected from the Precambrian crystalline basement bordering Gulf of Suez–Red Sea, along four sets of roughly east–west traverses (Fig. 1). Sample coordinates are given in Appendix 1. Fifty-six apatite fractions were successfully separated using conventional heavy liquid and magnetic techniques.

Fission track ages were measured using both the population method (PM; 16 samples) and the external detector method (EDM; 40 samples). Procedures, neutron dose calibrations and uncertainity of apatite ages dated by PM follow the methodology of Omar et al. [5]. Apatite fractions dated using EDM, and their muscovite detectors, were both etched at room temperature; apatite for 20–25 seconds in 5N HNO_3, and muscovite detectors for 25 minutes in 48% HF. Track counting was performed in transmitted light using a dry 80 × objective at a total magnification of 1250 × . All samples were irradiated in the RT-4 facility of the National Institute of Standards and Technology (NIST) reactor at Gaithersburg, Maryland. Thermal neutron doses were determined by counting tracks in muscovite detectors in contact with SRM-962a NIST standard glass, calibrated against NIST copper foil measurements [20]. In order to monitor flux gradients, two glass/mica dosimeters were included in each package irradiated. Individual fluences were determined by linear interpolation between the dosimeter glass values determined. Fish Canyon Tuff (FCT) apatite age standards (27.79 ± 1.4 m.y. [21]) were included and dated (using EDM) in each package as an additional check on fluence determinations. Ages calculated for FCT apatite standards in three irradiations using $\lambda_F = 7.03 \times 10^{-17}$ year^{-1}, range from 27.5 to 29 m.y. All samples dated by EDM passed the Chi-square test (at 5% level). Uncertainties of ages were determined by procedures described by Green [22].

TABLE 1

Fission-track analytical data for apatites from basement rocks bordering the western margin of the Gulf of Suez, Egypt

Sample No.	Altitude (m.a.s.l.)	ρ_s[a] ($\times 10^4$ tracks/cm^2)	ρ_i[a] ($\times 10^4$ tracks/cm^2)	Dose[b]	Number of grains[c]	$\bar{S}'$, χ^2[d]	Age[e] (m.y. $\pm 1\sigma$)	Mean length[f] $\pm$ st. error (μm)
E-161	550	62.99 (2173)	8.47 (766)	0.876	53/120	3.59%	379 ±23[p]	
E-155	550	230.10 (5580)	30.61 (1879)	0.881	35/79	3.83%	385 ±27[p]	12.72±0.17 (50)
UB-1	659	477.29 (1723)	627.70 (1133)	8.48	7	Pass	375 ±15	11.37±0.14 (100)
AH-1	602	207.56 (712)	318.54 (546)	9.59	6	Pass	364 ±21	11.77±0.15 (100)
UM-1	387	82.89 (527)	120.48 (383)	8.84	8	Pass	354 ±24	11.32±0.16 (100)
Z-1	250	454.34 (1020)	609.36 (684)	7.87	6	Pass	342 ±17	11.20±0.15 (100)
Z-2	300	347.59 (1286)	477.32 (883)	7.99	6	Pass	339 ±15	11.67±0.16 (100)
UM-6	505	175.17 (700)	250.74 (501)	8.12	7	Pass	331 ±20	10.47±0.15 (100)
AH-3	557	319.15 (1539)	578.98 (1396)	9.33	7	Pass	301 ±12	11.92±0.13 (100)
UM-4	488	96.17 (475)	158.34 (391)	8.35	6	Pass	297 ±21	10.98±0.15 (100)
AH-4	535	212.42 (1526)	393.66 (1414)	9.33	8	Pass	295 ±11	10.27±0.21 (100)
UM-3	427	93.80 (577)	161.60 (497)	8.60	9	Pass	292 ±18	10.44±0.16 (100)
E-249	500	54.19 (2071)	11.17 (657)	0.984	78/120	4.29%	280 ±20[p]	10.16±0.22 (75)
UM-2	425	113.26 (417)	209.14 (385)	8.6	6	Pass	273 ±20	11.75±0.16 (100)
KB-10	593	279.18 (1429)	538.20 (1382)	8.7	7	Pass	265 ±10	11.20±0.15 (50)
AH-2	604	127.86 (620)	285.00 (691)	9.59	6	Pass	253 ±14	9.44±0.19 (100)
HA-4	575	82.45 (385)	173.46 (405)	8.76	6	Pass	245 ±18	9.52±0.23 (50)
KB-5	435	189.31 (731)	431.96 (834)	9.17	7	Pass	236 ±12	10.56±0.25 (100)
KB-8	633	221.45 (875)	485.42 (959)	8.79	6	Pass	236 ±11	11.08±0.18 (50)
MA-5	840	89.73 (419)	186.32 (435)	8.14	6	Pass	230 ±16	10.60±0.27 (50)
HA-3	538	80.49 (298)	181.44 (334)	8.76	7	Pass	230 ±19	10.14±0.23 (50)
E-250	500	43.04 (2109)	11.31 (665)	0.984	100/120	5.19%	220 ±18[p]	9.48±0.27 (50)
KB-6	485	146.36 (874)	357.36 (1067)	8.98	9	Pass	216 ±10	11.30±0.14 (100)
UM-5	476	135.37 (778)	315.28 (906)	8.35	8	Pass	211 ±11	10.19±0.15 (100)
MA-2	334	119.01 (855)	292.60 (1051)	8.51	8	Pass	204 ±10	11.50±0.20 (50)
E-244	200	53.49 (1963)	15.76 (829)	0.984	106/120	5.48%	197 ±14[p]	11.20±0.25 (50)
KB-9	633	163.83 (765)	439.02 (1025)	8.79	7	Pass	193 ±10	11.44±0.17 (50)
KB-7	563	126.81 (911)	349.94 (1257)	8.98	8	Pass	192 ± 9	10.57±0.12 (100)
MA-6	633	101.39 (478)	296.10 (698)	8.14	6	Pass	165 ±10	10.50±0.23 (50)
UT-10	460	69.33 (386)	243.92 (679)	9.13	7	Pass	153 ±10	10.15±0.23 (100)
HA-2	401	76.86 (421)	303.78 (832)	8.95	8	Pass	134 ± 8	9.50±0.31 (50)
E-237	600	9.35 (550)	4.25 (250)	0.984	120/120	4.35%	128 ± 9[p]	
UT-1	204	63.19 (244)	290.56 (561)	9.87	6	Pass	127 ±10	9.96±0.33 (50)
MA-4	523	130.76 (728)	585.54 (1630)	8.32	8	Pass	110 ± 5	9.94±0.28 (50)
AH-5	489	123.32 (804)	707.42 (2306)	9.10	8	Pass	94 ± 4	11.04±0.28 (100)
E-248	525	15.77 (927)	9.54 (561)	0.984	120/120	4.59%	97 ± 7[p]	10.40±0.31 (50)
E-251	475	15.41 (906)	11.65 (685)	0.984	120/120	3.78%	77 ± 5[p]	9.30±0.34 (54)
E-247	525	9.68 (569)	7.53 (443)	0.984	120/120	3.99%	75 ± 5[p]	9.06±0.24 (50)
E-201	400	3.44 (202)	26.36 (1550)	0.984	120/120	2.96%	61 ± 4[p]	
E-240	500	8.55 (503)	7.70 (453)	0.984	120/120	5.22%	65 ± 5[p]	10.38±0.38 (34)
E-252	450	20.31 (1194)	18.38 (1081)	0.984	120/120	9.39%	65 ± 4[p]	
HA-1	411	26.76 (173)	257.36 (832)	8.95	8	Pass	55 ± 4.7	9.70±0.26 (100)
AH-7	442	17.93 (153)	174.66 (745)	8.84	11	Pass	54 ± 4.8	12.25±0.30 (100)
E-200	400	7.08 (416)	8.90 (523)	0.984	120/120	5.65%	47 ± 3.6[p]	10.68±0.25 (51)
UT-9	610	43.64 (290)	547.46 (1819)	9.13	8	Pass	43 ± 2.8	10.47±0.28 (100)
UT-8	790	36.63 (223)	662.90 (2018)	9.32	8	Pass	31 ± 2.2	11.81±0.25 (100)
UM-7	525	18.93 (135)	362.96 (1294)	8.12	10	Pass	25.3 ± 2.3	12.84±0.25 (98)
E-202	400	4.49 (264)	10.97 (645)	0.984	120/120	5.72%	24.1 ± 1.9[p]	12.89±0.24 (100)
UT-6	760	22.15 (175)	523.64 (2069)	9.50	10	Pass	24.0 ± 1.9	12.94±0.19 (100)
UT-7	610	14.32 (126)	334.54 (1472)	9.32	10	Pass	23.8 ± 2.2	12.41±0.25 (100)
AH-6	459	33.93 (262)	900.72 (3478)	9.10	10	Pass	20.5 ± 1.3	13.36±0.14 (100)
UT-2	310	13.06 (102)	404.22 (1579)	9.87	10	Pass	19.0 ± 2.0	13.52±0.16 (100)

TABLE 1 (continued)

Sample No.	Altitude (m.a.s.l.)	ρ_s[a] ($\times 10^4$ tracks/cm^2)	ρ_i[a] ($\times 10^4$ tracks/cm^2)	Dose[b]	Number of grains[c]	$\bar{S}'$, χ^2[d]	Age[e] (m.y. $\pm 1\sigma$)	Mean length[f] $\pm$st. error (μm)
E-203	425	11.55 (679)	36.57 (1971)	0.984	120/120	4.03%	18.6 ± 1.3[p]	13.14 ± 0.18 (100)
E-245	300	10.44 (614)	39.63 (2078)	0.984	120/107	4.32%	15.5 ± 1.2[p]	13.13 ± 0.20 (100)
UT-4	550	14.63 (88)	652.86 (1964)	9.69	8	Pass	13.0 ± 1.4	13.07 ± 0.16 (100)
UT-5	580	11.47 (103)	579.96 (2604)	9.5	10	Pass	11.2 ± 1.1	12.91 ± 0.20 (100)

[a] ρ_s = spontaneous track density; ρ_i = induced track density; brackets show number of tracks actually counted to determine the reported track density.

[b] $\times 10^{15}$ neutrons/cm^2.

[c] Different number of fields of view counted in determining the fossil track density (first number) and the induced track density (second number) for apatites dated by the population method. Single number indicates number of grains used in age determination by the external detector method.

[d] $\bar{S}'$ = relative standard error of the mean (%) for the induced-track count; χ^2 = test of variance.

[e] $\lambda_F = 7.03 \times 10^{-17}$ yr^{-1}, $I = 7.252 \times 10^{-3}$, $\sigma^{235} = 580.2 \times 10^{-24}$ cm^{-2}, $\lambda_D = 1.551 \times 10^{-10}$ yr^{-1}.

[f] Brackets show number of tracks measured.

[p] Apatite age determined by population method.

Length measurements were made on 52 apatite mounts prepared only for that purpose. Grains were etched for 20–25 seconds in 5*N* HNO_3 and measured using an 80 × dry objective at a total magnification of 1250 ×. Only horizontal confined track lengths (HCTL) with properties described by Gleadow et al. [23,24] were measured.

4. Results

Apatite FT analytical results and the areal distribution of FT ages are shown in Table 1 and Fig 1, respectively. Apatite FT ages obtained in this study fall in the range of ca. 11 to 385 m.y. (Fig. 1 and Table 1). Generally, young ages are found in the southern part of the study area and older ages in the north. Also, there is a crude correlation between apatite FT ages and distance from the rift margin, but there is considerable scatter. In fact, old ages often occur within very close geographic proximity to young ones.

HCTL measurements in most of the apatites studied are shown in Table 1.

5. Discussion

5.1. Interpretation of FT results

Apatite FT ages are substantially younger than their Precambrian host rocks. Phanerozoic magmatism in the area under investigation is minor. No samples were collected close to any of these magmatic bodies. Therefore, heat introduced by this small-scale, widely scattered and isolated magmatism, is not considered in the interpretation of apatite FT ages obtained in this study. Instead they are interpreted in the context of the regional cooling history of the basement rocks as a result of uplift and erosion.

Wagner [25] described track annealing in terms of three depth (temperature) zones (Fig. 3A). An uppermost total track stability zone (TSZ) in which all tracks are preserved; underlain by a partial annealing zone (PAZ) where tracks both accumulate and anneal; and finally a deeper total annealing zone (TAZ) where no tracks are recorded. Green et al. [26,27], reported that annealing of fission tracks occurs, although very slowly, even at ambient temperatures. This observation renders the TSZ concept technically invalid. However, because of the slow rate of annealing at temperatures corresponding to those of TSZ and the fact that fission-track ages have errors between 5 and 10%, the detectability of any age variation for samples residing in the TSZ will be beyond the resolution of the FT method. The use of the three-annealing-zones concept nonetheless remains a reasonable approximation to the true situation and will be used to interpret apatite FT data obtained in this study.

Theoretically, because of this annealing behaviour, apatites in crystalline basement rocks residing in the above mentioned zones under a stable thermal regime for a geologically long period of time, will record different age patterns. Apatites residing in the TSZ will record the oldest ages,

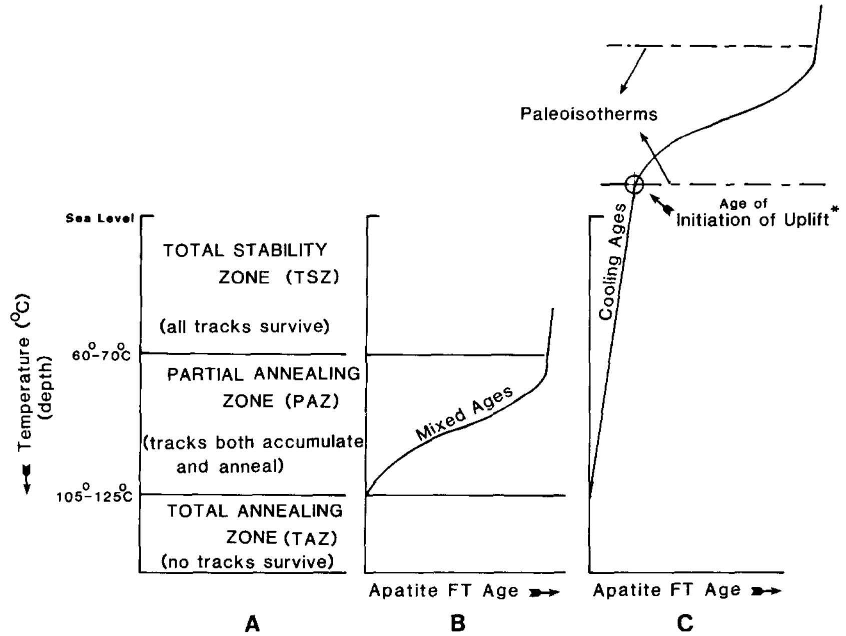

Fig. 3. Hypothetical profiles. A. The three fission track stability-related zones. Upper and lower temperature limits of the PAZ are for an effective heating time of 4×10^7 to 10^8 years (see text for more details). B. Apatite fission-track age versus temperature (depth) under stable thermal regime in the PAZ. C. Apatite fission-track age versus elevation after a period of cooling accompanying uplift and erosion. Paleoisotherms indicate upper and lower limits of the PAZ shown in B. Slope of cooling ages varies with rate of uplift; the greater the uplift rate the steeper the slope. *After correcting for annealing experienced during uplift to the surface (see discussion in text).

reflecting the original post-emplacement cooling of the basement host rocks. No tracks survive in apatites residing in the TAZ which will yield ages of zero. Apatites within the PAZ will record progressively younger ages with increasing temperature (depth) and attain an age of zero as the base of the zone is reached (Fig. 3B). Because of significant partial annealing in this zone, the "ages" have no direct relationship to geologic events and are termed "mixed" ages.

If the PAZ and the upper part of TAZ were brought to the surface as a coherent structural block by uplift and erosion, then apatite ages in the PAZ will increase with elevation (Fig. 3C). At the same time those apatites which resided in the TAZ would begin to record fission track ages. Because the latter are recorded during cooling accompanying uplift and erosion, they are conventionally called "'cooling" ages (Fig. 3C). The oldest apatite age in this group will be the closest to the timing of onset of uplift. However, this age will still be younger than the age of uplift initiation because of annealing experienced in the PAZ and TSZ while the sample ascended to the surface. Furthermore, because of the relatively large difference in residence time in the PAZ, the amount of annealing experienced by samples yielding "cooling ages" is much less than those recording "mixed" ages. Therefore, on an age/elevation plot, apatites recording "cooling" ages will form a line with a steeper slope than those yielding "mixed" ages (Fig. 3C). From the foregoing, it is clear that

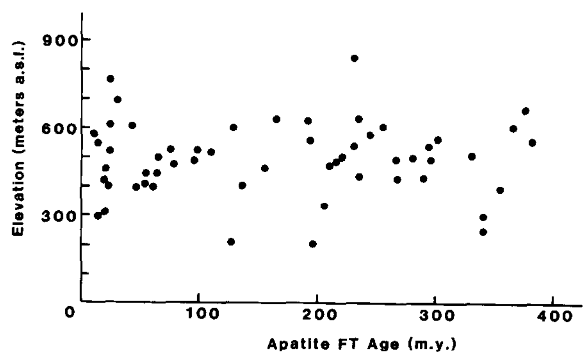

Fig. 4. Apatite fission-track age versus elevation for samples analyzed.

the break in slope on apatite/elevation plot can be used to date (after correcting for annealing experienced in the PAZ and TSZ, see discussion below) initiation of an uplift and erosion event (Fig. 3C). Such break points have been identified on apatite age/elevation plots in orogenic belts (e.g. [28,29]) and rifted margin uplifts (e.g. [6]).

In an uplift study in Sinai [30] and this study (Fig. 4), the apatite FT age/elevation relationship does not hold. Based on an apparent time-break between younger (< 26.6 m.y.) and older (> 90 m.y.) groups of apatite FT ages, Kohn and Eyal [30] arbitrarily proposed an age of 26.6 ± 3 m.y. for the onset of rift-related uplift in Sinai. The absence of an apatite FT age/elevation relationship (Fig. 4) coupled with the occurrence of older ages within very close geographic proximity to younger ones (Fig. 1) can be explained by assuming non-uniform uplift and differential motion between fault-bound blocks. This interpretation is in agreement with the structure of the study area which is dominated by NE-SW, NW-SE and N-S normal-fault sets [31].

A recent advance in the interpretation of FT ages with the aid of analysis of HCTL distributions permits more rigorous constraints to be placed on the meaning of an observed apatite age [23,24]. All fission tracks in a given mineral are nearly of the same length when formed. Fission tracks become progressively shorter during ther-

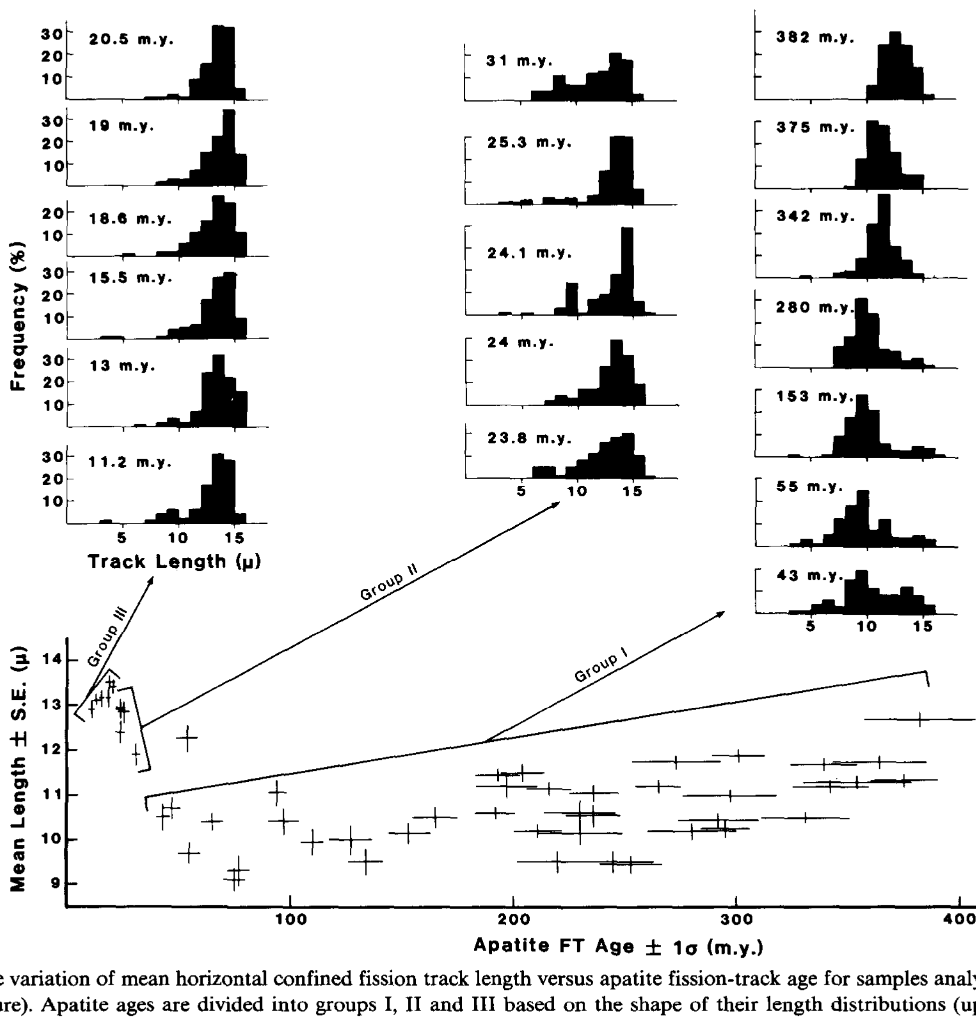

Fig. 5. The variation of mean horizontal confined fission track length versus apatite fission-track age for samples analyzed (lower part of the figure). Apatite ages are divided into groups I, II and III based on the shape of their length distributions (upper part of the figure) and their mean fission track length (see text for detailed discussion). Because of the large number of samples in group I, only representative samples are presented in this figure.

mal annealing, and, because each track is formed at a different time, it has been exposed to a different portion of the total thermal history of the sample. Analysis of HCTL distributions has proved to be a direct and unique way of differentiating between "mixed" and "cooling" FT ages of apatites which have experienced contrasting thermal histories. Apatites cooled from within the pre-uplift PAZ are mostly positively skewed and with increasing temperature show a progressive increase in the breadth of the length distributions and a steady decrease in mean track length. On the other hand, apatites cooled from the TAZ, yielding "cooling" ages, show a negatively skewed, narrow distributions of long tracks [23,24]. Apatites uplifted from levels near the bottom of the PAZ (highest degree of annealing) yield relatively broad length distributions consisting of either a small peak or a tail of short tracks, and a pronounced peak of long tracks. The former represent tracks which have undergone extensive shortening through prolonged exposure to near total annealing temperatures prior to uplift, while the latter represent relatively unannealed tracks which have accumulated subsequent to cooling.

On the basis of HCTL distribution and age, apatite samples studied here can be assigned to one of three distinct groups (Fig. 5).

Group I: Apatite ages ranging from 43 to 385 m.y. All apatites show positively skewed length patterns with the oldest age showing the narrowest distribution and longest mean length. As apparent apatite age decreases, HCTL distributions become progressively broader, with shorter mean length (Fig. 5 and Table 1). These data are typical of samples that have experienced significant partial annealing [23,24]. Hence, dates in this group are interpreted as "mixed" ages. Although there is a clear relationship between mean-length and apatite age in this group, the points show some scatter. This scatter may be due to anisotropy in the annealing of tracks [27] and differences in annealing properties of apatites as a function of their chemistry [27,32].

Group II: Apatite ages ranging from 23 to 31 m.y. All HCTL distributions are negatively skewed with either a distinct tail or a small peak of short tracks (Fig. 5). The presence of short tracks indicates that prior to uplift these apatites experienced extensive annealing at the bottom of the PAZ. Long tracks, constituting the right side of length distributions, accumulated during cooling. The mean-track length for these HCTL distributions show a negative correlation when plotted against their apatite ages (Fig. 5). The number of short tracks remaining in these apatites before final cooling is responsible for this relationship. The number of tracks accumulating in these apatites from the time of onset of cooling to the present is the same and these tracks are long. By contrast, the number of short tracks present in each apatite just before cooling depends on its relative position in the rock column near the base of the PAZ; the lower the sample in that column, the higher the temperature and fewer short tracks present. This situation creates an inverse relationship between mean-lengths and ages; a greater number of shortened tracks in apatite prior to uplift increases the age but decreases the mean length.

The above discussion indicates that samples in this group have resided for some period near the base of the PAZ where tracks formed prior to uplift were nearly totally annealed. Thus, apatite FT ages in this group are interpreted as "mixed" ages, older than the age of commencement of uplift. The base of the PAZ is difficult to identify on apatite age/elevation plots. However, this zone can be identified with certainty on apatite age/mean length plots. This demonstrates the importance of combining fission-track ages with track-length measurements.

Group III: Apatite ages ranging from 11 to 20.5 m.y. All HCTL distributions are unimodal, narrow and negatively skewed (Fig. 5). Mean-lengths for these samples are the longest among all samples analyzed in this study (Table 1) and slightly decrease with apatite FT age (Fig. 5). The small percentage of short tracks indicates that these samples have cooled relatively rapidly from within the TAZ. It follows from the above that the two oldest ages in this group (20.5 ± 1.3 and 19 ± 2 m.y.) are close to the timing of commencement of uplift in the study area. However, the mean lengths for these two samples, 13.36 and 13.52 μm, respectively, is less than those of "undisturbed volcanic-type" length distributions (about 15 μm) reported by Gleadow et al. [24]. Green [33], shows that a 1 : 1 relationship exists between reduction in track density (age) and reduction in mean length.

Therefore, these two ages postdate the timing of initiation of uplift in the study area. However, the approximate timing of onset of uplift can be obtained by correcting the ages of the two samples for annealing experienced during uplift from the base of the PAZ. This correction was carried out by calculating the age for each sample after the mean length of spontaneous tracks in that sample was normalized to that in an "undisturbed volcanic-type" length distribution. Because Fish Canyon Tuff apatite is used as an age standard, its measured spontaneous track mean length of 14.98 μm is used as the mean length of "undisturbed volcanic-type" length distribution. Applying the correction yields apatite ages of 23 ± 1.5 and 21 ± 2.2 m.y., respectively, for the two samples mentioned above. It is proposed that the initiation of rift-related uplift in the study area occurred between 21 ± 2.2 and 23 ± 1.5 m.y. ago. The virtual absence of a tail of short tracks in their length distribution implies relatively rapid uplift for these two samples. The sedimentary cover of the Gulf of Suez is presently eroding by scarp retreat. The escarpment lies 60–100 km west of the rift border faults for the southern half of the Gulf, thus averaging a horizontal retreat of 3–5 km/m.y. This erosional style, observed throughout the Red Sea and at a number of continental margins (e.g. southeastern Australia, southern Africa) could be responsible for the rapid cooling of basement rocks necessary for recording the early stage of uplift.

In Fig. 5, the two youngest apatite ages show a small tail or peak of short tracks indicating that they have experienced more partial annealing in the PAZ than apatites yielding older ages in this group. This might be attributed to one or a combination of the following possibilities: (1) and increase in the geothermal gradient, (2) episodic uplift, or (3) decrease in the erosion rate. These two samples could potentially have been the most affected by these factors because they occupied lower levels in the rock column during uplift than samples recording older apatite ages in this group. Possibility 2 is in good agreement with geologic evidence which indicates tectonic quiescence during the Middle Miocene (Fig. 2) [1–3]. Possibility 3 is suggested by the erosional style in the rift shoulder. The pre-rift sediments, removed by scarp retreat, erodes faster than the underlying more resistant basement, causing a slowing of the unroofing and cooling of the samples.

The previously outlined Phanerozoic history of sedimentation indicates that the basement studied here probably reached its maximum depth of burial about 40 m.y. ago. However, taking into account the prolonged period of gradually rising temperatures of basement rocks upon burial, we believe that a realistic pre-rift uplift heating time is of the order of 10^8 to 4×10^7 years. This heating time corresponds to temperatures of ca. 60–70 °C and 105–125 °C for the upper and lower temperature boundaries of pre-rift uplift PAZ, respectively [34,35].

Under initial geothermal gradients similar to that of the present-day average of about 21 °C/km [36], and assuming a surface temperature of 20 °C and 105–125 °C for total track annealing, about 4.6–5.5 km of vertical motion would be required to bring samples cooled from near the top of the pre-rift TAZ to their present-day elevation (ca. 500 m a.s.l.). Clearly, the vertical motion required is less for samples cooled from within the pre-rift PAZ and more for samples cooled from deep levels from the pre-rift TAZ. However, the actual amount of vertical motion is likely to be less because these calculations ignore the increase in geothermal gradient associated with the rifting process (e.g. [37]). Fission-track studies in southeast Egypt [5] and southeastern Australia [4] have shown that geothermal gradients during rifting could be double or more the present-day geothermal gradients in these areas. Furthermore, the "tectonic uplift", uplift in the absence of erosion, must have been less than 4.6–5.5 km because erosion of uplifted crust unloads the surface causing regional isostatic uplift [38]. Detailed estimates of "tectonic uplift" will be reported elsewhere.

5.2. *Implications for rifting processes*

Geological evidence from the Gulf of Suez region show that rift faulting and volcanism was already underway by the end of the Oligocene/earliest Miocene [8]. Analyses of the subsidence in the Gulf of Suez show that, following a slow period of rift initiation, the deposition of the Rudeis Formation marks a rapid phase of extension. Age estimates of the beginning of the Rudeis deposition, showing the most rapid subsidence and greatest water depths, range from 19 to 21 m.y. [1–3,14]. The FT estimates of the initiation of rift-flank uplift of the Gulf of Suez (21–23 m.y.), obtained by length-correcting the samples, either

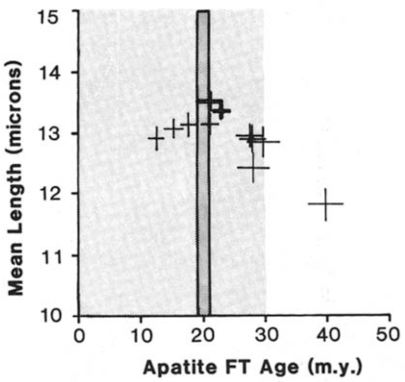

Fig. 6. Detail of the extreme left of the lower part of Fig. 5. In this plot the apatite FT ages have been corrected for the reduction in age that accompanies track length shortening (see text). The light shading indicates the time period of rifting [8] and the bar spanning 19–21 m.y. marks the beginning of the main phase of extension [1–3,14] in the Gulf of Suez. The two FT ages represented by boldface crosses indicate that rift-flank uplift at the Gulf of Suez began 21–23 m.y. ago.

coincides with the start of this period or slightly predates it. Fig. 6 shows the correlation of the tectonic transition in the Gulf of Suez to the FT results. The FT data indicate a direct relationship between the uplift and extension histories in the Gulf of Suez rift.

These results firmly support recent interpretations of the regional geology on the absence of a major pre-rift doming phase [8,10,11,38,39]. The rift geometry was already established [8] prior to uplift to the rift flanks. Thus, the initiation of the Gulf of Suez by an active rifting process involving asthenospheric heat source as the driving force for rifting can be ruled out. Rather, the development of large rift flank uplift along the Gulf of Suez and the northern Red Sea is contemporaneous with, and is directly related to, the process of extension.

Processes which can cause rift flank uplift in passive rifts include: lateral transfer of heat due to conduction [40]; increased heat transfer due to small-scale convection [41]; flexural response to tectonic denudation [42]; and viscous flow due to extension [43]. Our results support those models of rift process which lead to contemporaneous uplift and subsidence such as flexure and viscous flow in response to extension. The area of uplift is broad, with up to 1 km of tectonic uplift as far as 80 km from the coast on the southern line of samples. This is consistent with the model of small-scale convection under rifts and with the flexure model. However, for flexure to be the sole cause of the uplift requires large flexural rigidities during rifting. Furthermore, flexure acts only to redistribute the uplift and subsidence across a rift. The total amount of uplift at the Gulf of Suez is greater than can be generated by passive rifting and requires the addition of extra heat such as due to small scale convection [11].

6. Conclusions

(1) The basal portion of the PAZ for uplifted basement rocks can be identified on apatite FT age/mean length plots.

(2) The initiation of the basement uplift along the western margin of the Gulf of Suez took place between 21 and 23 m.y. ago.

(3) Commencement of this uplift is contemporaneous with, and is directly related to, the processes of extension and subsidence at the Gulf of Suez.

Acknowledgements

We would like to thank Shawkey Abdine of GUPCO and Chris Heath at Amoco Egypt for their support of our fieldwork. Special thanks are due to Mosbah Khalil and Hussein Fouda who guided our fieldwork, and Mahmoud and Hassan, our drivers. A special debt of gratitude is due to Dr. S. Carpenter of NIST for supervising neutron irradiations. The manuscript was greatly improved by review from Drs. I. Harker, G. Karner, T. Lutz, C.W. Naeser and an anonymous reviewer. This research was supported by National Science Foundation grant OCE-86-10213 and Gas Research Institute contract GRI 5087-260-1546.

References

1 I. Moretti and B. Colletta, Spatial and temporal evolution of the Suez rift subsidence, Geodynamics 7, 151–168, 1987.
2 M.S. Steckler, F. Berthelot, N. Lyberis and X. Le Pichon, Subsidence in the Gulf of Suez: implications for rifting and plate kinematics, Tectonophysics 153, 249–270, 1988.
3 M. Richardson and M.A. Arthur, The Gulf of Suez–northern Red Sea Neogene rift: a quantitative basin analysis, Mar. Pet. Geol. 5, 247–270, 1988.
4 M.E. Moore, A.J.W. Gleadow and J.F. Lovering, Thermal evolution of rifted continental margins: new evidence from

Appendix 1

Sample localities

Sample No.	Latitude (N)	Longitude (E)	Sample No.	Latitude (N)	Longitude (E)
E-161	27°34.0′	32°56.0′	MA-6	27°35.4′	33°04.0′
E-155	27°34.0′	32°34.0′	UT-10	26°30.4′	33°18.8′
UB-1	27°47.5′	32°45.7′	HA-2	28°24.0′	32°38.7′
AH-1	28°09.0′	32°29.8′	E-237	27°01.2′	33°36.7′
UM-1	28°37.1′	32°32.2′	UT-1	26°44.0′	33°52.4′
Z-1	27°59.0′	33°28.0′	MA-4	27°34.4′	33°04.7′
Z-2	27°56.1′	33°30.1′	AH-5	28°14.0′	32°40.8′
UM-6	28°34.2′	32°26.2′	E-248	28°18.5′	32°35.3′
AH-3	28°11.0′	32°37.1′	E-251	28°24.0′	32°37.8′
UM-4	28°37.2′	32°28.5′	E-247	28°20.2′	32°33.0′
AH-4	28°12.3′	32°39.3′	E-201	26°41.5′	33°45.8′
UM-3	28°36.8′	32°30.0′	E-240	26°58.0′	33°29.7′
E-249	28°22.3′	32°24.0′	E-252	28°22.3′	32°39.7′
UM-2	28°36.7′	32°30.7′	HA-1	28°25.4′	32°40.1′
KB-10	27°45.0′	32°48.5′	AH-7	28°17.8′	32°43.8′
AH-2	28°10.6′	32°34.1′	E-200	26°44.5′	33°52.5′
HA-4	28°16.7′	32°29.3′	UT-9	26°35.2′	33°25.5′
KB-5	27°42.6′	32°57.9′	UT-8	26°39.0′	33°30.2′
KB-8	27°43.3′	32°51.2′	UM-7	28°33.6′	32°24.9′
MA-5	27°35.6′	33°03.6′	E-202	26°41.7′	33°44.7′
HA-3	28°18.3′	32°32.0′	UT-6	26°41.7′	33°35.9′
E-250	28°20.7′	32°37.8′	UT-7	26°39.5′	33°33.9′
KB-6	27°42.7′	32°55.2′	AH-6	28°16.5′	32°42.4′
UM-5	28°36.2′	32°27.2′	UT-2	26°41.5′	33°49.8′
MA-2	27°35.2′	33°09.1′	E-203	26°42.3′	33°39.8′
E-244	27°33.8′	33°28.5′	E-245	27°43.7′	33°00.0′
KB-9	27°43.0′	32°50.4′	UT-4	26°42.0′	33°42.3′
KB-7	27°42.2′	32°52.6′	UT-5	26°42.2′	33°39.4′

fission tracks in basement apatites from southeastern Australia, Earth Planet. Sci. Lett. 78, 255–270, 1986.

5 G.I. Omar, B.P. Kohn, T.M. Lutz and H. Faul, The cooling history of Silurian to Cretaceous alkaline ring complexes, south Eastern Desert, Egypt, as revealed by fission-track analysis, Earth Planet. Sci. Lett. 83, 94–108, 1987.

6 A.J.W. Gleadow and P.G. Fitzgerald, Uplift history and structure of the Transantarctic Mountains: new evidence from fission track dating of basement apatites in the Dry Valleys area, Southern Victoria Land, Earth Planet. Sci. Lett. 82, 1–14, 1987.

7 R. Said, The Geology of Egypt, 377 pp., Elsevier, Amsterdam, 1962.

8 Z. Garfunkel and Y. Bartov, The tectonics of the Suez rift, Geol. Surv. Israel Bull. 71, 44 pp., 1977.

9 B.W. Sellwood and R.E. Netherwood, Facies evolution in the Gulf of Suez area: sedimentation history as an indicator of rift initiation and development, Modern Geol. 9, 43–69, 1984.

10 P.Y. Chenet and J. Letouzey, Tectonics of the area between Abu-Durba and Gebel Mezzazt (Sinai, Egypt) in the context of the evolution of the Suez rift, Bull. Cent. Rech. Explor. Brod. Elf-Aquitaie 7, 201–215, 1983.

11 M.S. Steckler, Uplift and extension at the Gulf of Suez: indications of induced mantle convection, Nature 317, 135–139, 1985.

12 P.R. Vail, R.M. Mitchum, Jr., R.G. Todd, J.M. Widmier, S. Thompson, III, J.B. Sangree, J.N. Bubb and W.G. Hatelid, Seismic stratigraphy and global changes of sea level, in: Seismic Stratigraphy—Application to Hydrocarbon Exploration, C.E. Clayton ed., Am. Assoc. Pet. Geol. Mem. 26, 49–212, 1977.

13 B.U. Haq, J. Hardenbol and P.R. Vail, Chronology of fluctuating sea levels since the Triassic, Science 235, 1156–1167, 1987.

14 R.W. Scott and F.M. Govean, Early depositional history of a rift basin: Miocene in western Sinai, Palaeogeogr., Palaeoclimatol., Palaeoecol. 52, 143–158, 1985.

15 A.L. Evans and I.W. Moxon, Gebel ZEIT chronostratigraphy: Neogene syn-rift sedimentation atop a long-lived palaeohigh, Proc. 8th E.G.P.C. Exploration Seminar, Cairo, 1986.

16 A.L. Evans, Neogene tectonic and stratigraphic events and in the Gulf of Suez rift area, Egypt, Tectonophysics 153, 235–248, 1988.

17 M.S. Steckler and U.S. ten Brink, Lithospheric strength

variations as a control on new plate boundaries: examples from the northern Red Sea region, Earth Planet. Sci. Lett. 79, 120–132, 1986.

18 C. Mc. Serencsits, H. Faul, K.A. Foland, A.A. Hussein and T.M. Lutz, Alkaline ring complexes in Egypt: Their ages and relationship in time, J. Geophys. Res. 86, 3009–3013, 1981.

19 R. Ressetar, A.E.M. Nairn and J.R. Monard, Two phases of Cretaceous–Tertiary magmatism in the Eastern Desert of Egypt: palaeomagnetic, chemical and K/Ar evidence, Tectonophysics 13, 169–193, 1981.

20 B.S. Carpenter, Standard reference materials: calibrated glass standards for fission-track use, Natl. Bur. Stand. Spec. Publ. 260, 12 pp., 1984.

21 M.J. Kunk, J.F. Sutter and C.W. Naeser, High precision $^{40}Ar/^{39}Ar$ ages of sanidine, biotite, hornblende and plagioclase, from the Fish Canyon Tuff, San Juan volcanic field, south-central Colorado, Geol. Soc. Am., Abstr. Prog. 17, 636, 1985.

22 P.F. Green, A new look at statistics in fission track dating, Nucl. Tracks 5, 77–86, 1981.

23 A.J.W. Gleadow, I.R. Duddy, P.F. Green and K.A. Hegarty, Fission track lengths in the apatite annealing zone and the interpretation of mixed ages, Earth Planet. Sci. Lett. 78, 245–254, 1986.

24 A.J.W. Gleadow, I.R. Duddy, P.F. Green and J.F. Lovering, Confined fission track lengths in apatite: a diagnostic tool for thermal history analysis, Contrib. Mineral. Petrol. 94, 405–415, 1986.

25 G.A. Wagner, Correction and interpretation of fission track ages, in: Lectures in Isotope Geology, E. Jäger and J.C. Hunziker, eds., pp. 170–177, 1979.

26 P.F. Green, I.R. Duddy, A.J.W. Gleadow, P.T. Tingate and G.M. Laslett, Fission-track annealing in apatite: track length measurements and the form of the Arrhenius plot, Nucl. Tracks 10, 323–328, 1985.

27 P.F. Green, I.R. Duddy, A.J.W. Gleadow, P.R. Tingate and G.M. Laslett, Thermal annealing of fission tracks in apatite, 1. A qualitative description, Chem. Geol. Isot. Geosci. Sect. 59, 237–253, 1986.

28 C.W. Naeser, Fission-track dating and geologic annealing of fission tracks: in: Lectures in Isotope Geology, E. Jäger and J.C. Hunziker, eds., pp. 154–169, 1979.

29 G.A. Wagner, G.M. Reimer and E. Jäger, Cooling ages derived by apatite fission-track, mica Rb/Sr and K/Ar dating: the uplift history of the central Alps, mem. Ist. Geol. Mineral. Univ. Padova 30, 1–27, 1977.

30 B.P. Kohn and M. Eyal, History of uplift of the crystalline basement of Sinai and its relation to opening of the Red Sea as revealed by fission track dating of apatites, Earth Planet. Sci. Lett. 52, 129–141, 1981.

31 M. Ghanem, A.A. Dardir, M.H. Francis, A.A. Zalata and K.M. Abu Zeid, Basement rocks in Eastern Desert of Egypt North of Latitude 26°40′N, Ann. Geol. Surv. Egypt III, 33–38, 1973.

32 K.D. Crowley and M. Cameron, Annealing of etchable fission-track damage in apatite: effects of anion chemistry, Geol. Soc. Am., Abstr. Prog. 19, 631, 1987.

33 P.F. Green, The relationship between track shortening and fission track age reduction in apatite: combined influences of inherent instability, annealing anisotropy, length bias and system calibration, Earth Planet. Sci. Lett. 89, 335–352, 1988.

34 C.W. Naeser, The fading of fission tracks in the geologic environment, Nucl. Tracks 5, 248–250, 1981.

35 A.J.W. Gleadow and I.R. Duddy, A natural long term experiment for apatite, Nucl. Tracks 5, 169–174, 1981.

36 P. Morgan, F.K. Boulos, S.F. Hennin, A.A. El-Sheriff, A.A. El-Sayed, N.Z. Basta and Y.S. Melek, Heat flow in eastern Egypt: the thermal signature of a continental breakup, J. Geodyn. 4, 107–131, 1985.

37 T.L. Thompson, Plate tectonics in oil and gas exploration of continental margins, Am. Assoc. Pet. Geol. Bull. 60, 1463–1501, 1976.

38 Z. Garfunkel, Relation between continental rifting and uplifting: evidence from the Suez rift and northern Red Sea, Tectonophysics 150, 33–50, 1988.

39 R.G. Bohannon, C.W. Naeser, D.L. Schmidt and R.A. Zimmermann, The timing of uplift, volcanism, and rifting peripheral to the Red Sea: A case for passive rifting?, J. Geophys. Res. 94, 1683–1701.

40 M.S. Steckler and A.B. Watts, The Gulf of Lion: subsidence of a young continental margin, Nature 287, 425–429, 1980.

41 W.R. Buck, Small-scale convection induced by passive rifting: the cause for uplift of rift shoulders, Earth Planet. Sci. Lett. 77, 362–372, 1986.

42 J.K. Weissel and G.D. Karner, Flexural uplift of rift flanks due to tectonic denudation of the lithosphere extension, J. Geophys. Res., in press, 1988.

43 M.T. Zuber and E.M. Parmentier, Lithospheric necking: a dynamic model for rift morphology, Earth Planet. Sci. Lett. 77, 373–383, 1986.